RSC Advances

ROYAL SOCIETY OF CHEMISTRY

www.rsc.org/advances

Abstract:

This work predicts the elastic modulus tensor, equation of state, and coefficients of thermal expansion at all stable thermodynamic states for γ-RDX. The work provides substantial material information for continuum modeling of RDX.

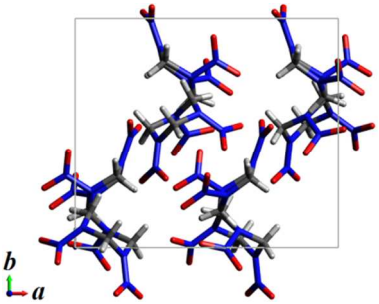

Journal Name

RSCPublishing

ARTICLE

Thermomechanical properties and equation of state for the γ-polymorph of hexahydro-1,3,5-trinitro-1,3,5-triazine

Cite this: DOI: 10.1039/x0xx00000x

Kartik Josyula,[a] Rahul[a] and Suvranu De*[a]

Received ooth January 2012,
Accepted ooth January 2012

DOI: 10.1039/x0xx00000x

www.rsc.org/

The thermomechanical properties of the γ-polymorph of hexahydro-1,3,5-trinitro-1,3,5-triazine (RDX) are predicted using a non-reactive fully flexible Smith and Bharadwaj molecular potential using molecular dynamics simulations. The elastic modulus tensor, coefficients of thermal expansion, and lattice constants are calculated as functions of pressure (4-11GPa) and temperature (200-550K). Much like α-RDX, the components of the elastic modulus tensor of γ-RDX are found to increase monotonically with pressure, but soften only mildly with increase in temperature. Another interesting observation is that the b-lattice parameter is insensitive to temperature changes and is almost unchanged at higher pressures. A third order Birch-Murnaghan equation of state and the coefficients of thermal expansion are obtained from the pressure-volume-temperature (pVT) data. Around the α-γ phase transition pressure, the coefficients of thermal expansion for γ-RDX are greater than those of α-RDX. In contrast to α-RDX, the coefficients of thermal expansion for γ-RDX exhibit negligible variation with pressure. The predicted values of the thermomechanical properties and crystal parameters agree reasonably well with experimental results and other molecular simulations reported in literature.

1. Introduction

While experiments and field-testing are necessary, modeling and simulation are indispensable in determining detailed mechanisms that affect the sensitivity of energetic materials including hexahydro-1,3,5-trinitro-1,3,5-triazine (RDX). In recent years, there has been an increased interest in understanding and predicting the macroscopic response of RDX on the basis of thermomechanical properties that are required in the formulation and parameterization of the mesoscale continuum mechanical constitutive models.[1,2] In particular, these thermomechanical properties are needed as functions of pressure and temperature in order to capture shock phenomena in RDX.[1] At high loading rates, the pressure gradients cause gradients in the elastic constants in the pressured and non-pressured regions of the material. This results in gradients in the wave speed. With increasing loading rates, the gradient in the wave speed behind and after the wave front leads to a stress singularity in the form of a shock. Thus, to appropriately capture the physics of high loading rates, the evolution of the material parameters, especially the elastic tensor, with pressure and temperature must be incorporated into the model.[1,3-5] Further, the pressure and temperature dependent thermomechanical properties of high-pressure γ-polymorph of RDX are needed for the modeling of shock induced α-γ phase transformation in RDX. While thermomechanical parameters of the most stable α-polymorph of RDX are reported in the literature,[6-11] it is not as easily found in the open literature for the high-pressure γ-polymorph, which may play an important role in the detonation mechanism of RDX.[12-14] More details on the factors influencing detonation properties and sensitivity of energetic materials may be found elsewhere.[15-18] In this paper, we report the thermomechanical properties and pVT equation of state for γ-RDX as functions of temperature and pressure using non-reactive fully flexible molecular potential and molecular dynamics simulations.

The crystal structure of α-RDX has been determined as orthorhombic using X-ray diffraction experiments.[19] It belongs to the *Pbca* space group with eight molecules occupying the eight lattice sites. The elastic modulus tensor of α-RDX is measured experimentally using Resonant Ultrasound Spectroscopy (RUS),[6] Brillouin scattering,[7] and Impulsive Stimulated Thermal Scattering (ISTS).[8] While the measurements from RUS and ISTS are within comparable range, the ones from Brillouin scattering are much higher, although indicating similar qualitative features. The coefficients

[a] *Department of Mechanical, Aerospace, and Nuclear Engineering, Rensselaer Polytechnic Institute, Troy, New York, 12180, USA. E-mail: des@rpi.edu*

of thermal expansion are calculated experimentally using a thermal analyzer and a thermo-mechanical analyzer.[20] Plate impact shock experiments[13,21,22] on α-RDX show anisotropic response with anomalous hardening for certain shock directions. Molecular dynamics simulations using the Smith and Bharadwaj (SB) potential[23] are able to replicate the experimental crystal structure of α-RDX along with elastic tensor modulus with good accuracy.[24] The same potential has been successfully used to simulate a delayed plastic response when the crystal was shocked normal to (111) and (021) planes in large scale molecular dynamics simulations.[21,22] Hugoniostat simulations using the same potential predict the Hugoniot elastic limit for shocks along [100] direction.[25] Monte-Carlo simulations using a rigid molecular potential[26] have simulated material properties like elastic moduli, pressure-volume-temperature (pVT) equation of state, coefficients of thermal expansion, and volumetric compression ratio for a wide range of pressures and temperatures for α-RDX.[9]

RDX undergoes a reversible phase transition to the γ-polymorph at around 3.8 GPa hydrostatic pressure in the temperature range of 150 K to 375 K.[27,28] The α-γ phase transition involves a decrease in unit cell volume of about 3% and leads to changes in the space group and molecular conformations.[29] The crystal structure is determined as orthorhombic at T = 300 K and P = 5.2 GPa using high pressure X-ray and neutron diffraction. It belongs to the $Pca2_1$ (alternatively $Pb2_1a$) space group with two molecules at each of the four lattice sites.[29] The lattice constants and a third order Birch Murnaghan equation of state have also been proposed.[29] Raman spectroscopic analysis of RDX crystals shocked along different directions suggests that the α-γ phase transition occurred around a peak stress of 5.5 GPa irrespective of direction of shock load.[12] Raman spectroscopy and optical imaging provide a complete description of the pressure-temperature conditions for decomposition of γ-RDX.[14] Molecular dynamics simulations using the SB potential accurately predict the crystal structure and lattice constants of γ-RDX at 300 K and 5.2 GPa[24] in accord with the experimental results.[29] The simulations have estimated the elastic modulus tensor at the similar conditions.[24] The hydrostatic compression simulations show phase transition in one direction only, namely, γ to α at about 2.1 GPa. However, the uniaxial compression simulation along [001] direction, results in bi-directional phase transition between α and γ polymorphs.[24] Hugoniostat simulations, using the same potential, observe similar bi-directional phase transitions for uniaxial compressions along [001].[25]

In this paper, we perform molecular dynamics simulations using a non-reactive fully flexible Smith and Bharadwaj molecular potential to compute the thermomechanical properties of γ-RDX. The elastic modulus tensor, coefficients of thermal expansion, and equation of state for γ-RDX are calculated as functions of pressure and temperature ranging from 4 GPa to 11 GPa and 200 K to 550 K, respectively. The equilibration and pVT data are collected using an isothermal-isostress ensemble (NσT) in which each component of the stress tensor is controlled individually. The elastic modulus tensor is calculated using an isothermal-isochoric ensemble (NVT).

This paper is organized as follows. In Section 2, we briefly discuss the molecular potential used in this study, followed by the simulation procedure. The thermomechanical properties and pVT equation of state for γ-RDX as a function of pressure and temperature are presented in Section 3. Finally, conclusions and comments on possible avenues for future work are presented in Section 4.

2. Methods

The results are obtained using molecular dynamics (MD) simulations in both the isothermal-isochoric (NVT) and isothermal-isostress (NσT) ensembles. In Section 2.1, we briefly discuss the molecular potential that is used for the simulation, followed by details of the simulation methodology in Section 2.2.

2.1 Molecular Potential

The present analysis does not deal with any reaction or decomposition of RDX. Hence, the non-reactive Smith and Bharadwaj (SB) potential[23] is used to model the fully flexible bonded interactions and the electrostatic, dispersion, and repulsion forces between the non-bonded atoms. The SB potential has not been fitted for any properties of condensed phase cyclic nitramines like RDX or Octahydro-1,3,5,7-tetranitro-1,3,5,7-tetrazocine (HMX). However, it has been found to reproduce many properties and phenomena for RDX and HMX in various atomistic simulations.[30,31] The SB potential used for the present simulations is of the form,

$$U = \sum_{\text{bonds}} \frac{1}{2} K_{ij}^{S} (r_{ij} - r_{ij}^{0})^2 + \sum_{\text{angles}} \frac{1}{2} K_{ijk}^{B} (\theta_{ijk} - \theta_{ijk}^{0})^2 \quad (1)$$
$$+ \sum_{\substack{\text{proper} \\ \text{dihedrals}}} \frac{1}{2} K_{ijkl}^{T} \left[1 - \cos(n\varphi_{ijkl})\right] + \sum_{\substack{\text{improper} \\ \text{dihedrals}}} \frac{1}{2} K_{ijkl}^{D} \varphi_{ijkl}^{2}$$
$$+ \sum_{i=1}^{N-1} \sum_{j>i}^{N} \left(A_{ij} \exp(-B_{ij} r_{ij}) - \frac{C_{ij}}{r_{ij}^{6}} + k_e \frac{q_i q_j}{r_{ij}} \right)$$

The intramolecular potentials for bonds (K^S, r^0), angles (K^B, θ^0), proper dihedrals (K^T, n), and improper dihedrals (K^D) are modeled as harmonic. The non-bonded interactions consist of Buckingham style potential with an exponential decay for repulsion (A, B) and $1/r^6$ decay for dispersion (C), and the Coulombic electrostatic potential (k_e). The Ewald summation method is used for the long-range interactions with a relative error tolerance of $1x10^{-4}$. The parameters and adjustments that are used in this study are described elsewhere in the literature.[31,32]

2.2 Simulation Method

Molecular dynamics (MD) simulations in the isothermal-isochoric (NVT) and isothermal-isostress (NσT) ensembles were performed using the LAMMPS (Large-scale Atomic/Molecular Massively Parallel Simulator) computer

code.[33] The unit cell of γ-RDX is constructed using crystallographic properties, atomic positions and molecular configuration details characterized by Davidson et al.[29] γ-RDX is modeled in the $Pb2_1a$ space group to provide direct comparison with the α-polymorph. The cut off distance of non-bonded van der Waals and electrostatic interaction forces is taken as 10 Å so that the nearest neighbouring molecules can interact with each other. This, in turn, dictates the length of the simulation box to be at least twice that of the cut off distance. Hence, the unit cell is replicated 2x3x3 times in each of the coordinate directions to create a simulation box containing 3024 atoms and 144 molecules. The simulation box has non-orthogonal periodic boundary conditions in all three directions so as to facilitate the simulation of bulk phenomena along with shear analyses. Time integration is performed using the standard velocity Verlet algorithm. For a stable simulation, a timestep of 0.75 fs is used. The time constants for the thermostat and barostat in the NσT and NVT ensembles are set to 1.0 ps.

The simulation box is warmed up for 7.5 ps, during which the temperature is reset to 300 K at every 5 steps using velocity scaling in an NσT ensemble at 5.2 GPa pressure. This is the pressure at which the crystal structure of γ-RDX was determined experimentally.[29] It is then equilibrated for 75 ps using NσT ensemble at 300 K temperature and 5.2 GPa pressure. The crystallographic dimensions, pressure, temperature, volume, and six components of stress tensor of the system are recorded during the equilibration process, as the system is stable during this process. No data are recorded during the warm-up process. In order to perform elastic modulus tensor analysis at various pressures and temperatures, pressure is incremented (or decremented) in steps of 0.5 GPa if the desired pressure is less than 8 GPa, and in steps of 1 GPa if the desired pressure is greater than or equal to 8 GPa, followed by temperature increment in steps of 50 K. At every increment the system is equilibrated for 75 ps.

The pressure, temperature, and volume of the system collected during the equilibration process, describe the equation of state for the system. Further, analyzing the deformation along each dimension during the temperature increment at a given pressure provides the coefficient of thermal expansion.

The elastic modulus tensor analysis is performed using a NVT ensemble. The components of elasticity tensor are calculated by applying strain fields along the three normal and shear directions in increments of 0.1% to a total of 1% and equilibrating the system at a desired pressure and temperature. The desired strain at each increment is applied to the simulation box. Each molecule is translated as a whole by a scaled displacement calculated using deformation gradient tensor $\boldsymbol{F}$, which is expressed in terms of lattice vectors as

$$\boldsymbol{F} = \boldsymbol{h}\boldsymbol{h}_0^{-1}, \quad (2)$$

where $\boldsymbol{h_o}$ and $\boldsymbol{h}$ are the matrices containing column-wise lattice vectors before and after enforcing the strain field, respectively. The center of mass of a molecule, initially present at position $\boldsymbol{x_o}$, is mapped to the final position,

$$\boldsymbol{x} = \boldsymbol{F}\boldsymbol{x}_0. \quad (3)$$

In this way, the molecule is not strained internally. The system is then thermalized for 75 ps at the desired temperature using a NVT ensemble. The Lagrangian strain ($\boldsymbol{E}$) corresponding to the deformation field is

$$\boldsymbol{E} = \frac{1}{2}(\boldsymbol{F}^T\boldsymbol{F} - \boldsymbol{I}) = \frac{1}{2}(\boldsymbol{h}_0^{-T}\boldsymbol{h}^T\boldsymbol{h}\boldsymbol{h}_0^{-1} - \boldsymbol{I}), \quad (4)$$

where $\boldsymbol{I}$ is the identity matrix. For small deformations, the work conjugate stress is defined by the constitutive equation through elastic modulus tensor $\boldsymbol{C}$ as,

$$\boldsymbol{\sigma} - \boldsymbol{\sigma}_0 = \boldsymbol{C} : \boldsymbol{E}, \quad (5)$$

where $\boldsymbol{\sigma}_0$ is the stress before the strain is applied. At the end of the process, the desired stress components are measured, and the slopes of the stress- strain curves provide the corresponding components of the elastic tensor.

3. Results and Discussion

The Smith and Bharadwaj non-reactive fully flexible molecular potential is used to perform molecular dynamics simulations on crystalline γ-RDX in order to calculate the orthotropic elastic modulus tensor. The system is equilibrated and pVT data is collected using the isothermal-isostress (NσT) ensemble. The elastic modulus tensor is calculated by applying a strain field in the three normal and shear directions and stabilizing the system in the isothermal-isochoric (NVT) ensemble. The equation of state and coefficients of thermal expansion are obtained from the pVT data.

The γ-RDX system is initially equilibrated at 5.2 GPa and 300 K and then elastic moduli are calculated at pressures corresponding to 4 GPa to 11 GPa in increments of 1 GPa. At each pressure, the temperature range for stable γ-polymorph is obtained from the phase diagram of RDX.[14] The pressure and temperature ranges for which elastic tensor moduli are calculated, is shown in Table 1.

Table 1 Pressure and temperature ranges for stable γ-RDX

Pressure Range (GPa)	Temperature Range (K)
4	200 – 450
5 – 7	200 – 500
8 – 11	200 – 550

At each pressure, the elastic modulus tensor is calculated, starting at 200 K in increments of 50 K.

In Section 3.1, we present the simulation results for the elasticity tensor of γ-RDX along with its variation with pressure and temperature followed by a comparison with α-RDX. In Section 3.2, we present the parameters of the equation of state, and coefficients of thermal expansion for γ-RDX with a comparative study of the thermal properties of α-RDX and γ-RDX. A discussion on the results is presented in Section 3.3.

3.1 Pressure and Temperature Variation of the Elasticity Tensor of γ-RDX

Table 2 presents the components of the elasticity tensor of γ-RDX at 5.2 GPa and 300 K, which are seen to compare reasonably well with the results previously reported by Munday et al.[24] The simulation protocol followed here is similar to

Munday et al.,[24,32] except for the different increments in temperature.

Table 2 Elastic modulus tensor for γ-RDX at 5.2 GPa and 300 K

(GPa)	Munday et al.[a]	Calculated
C_{11}	80.3	78.2
C_{22}	67.0	67.4
C_{33}	57.9	57.2
C_{32}	43.9	44.7
C_{31}	37.0	33.6
C_{21}	37.8	37.2
C_{44}	11.9	12.1
C_{55}	16.3	16.1
C_{66}	13.4	13.1

[a] Reference 24

The elastic constants of γ-RDX are generally larger than those of α-RDX,[6,7,8,9] indicating an overall stiffer response for the former. For both polymorphs, the C_{11} elastic constant is the largest, suggesting strongest intermolecular interactions along *a*-lattice. For γ-RDX, the elastic constants $C_{11}>C_{22}>C_{33}$, indicating elastic anisotropy similar to α-RDX.

We next calculate the elastic modulus tensor for the pressure ranging from 4 GPa to 11 GPa and for the temperature range as shown in Table 1. The components of the elasticity tensor are enlisted in Table 3 with respective temperatures and pressures. Figs. 1 and 2 depict the variation of the elastic moduli with pressure and temperature, respectively.

Table 3 Pressure and temperature variation of elastic modulus tensor for γ-RDX

P (GPa)	T (K)	C_{11} (GPa)	C_{22} (GPa)	C_{33} (GPa)	C_{32} (GPa)	C_{31} (GPa)	C_{21} (GPa)	C_{44} (GPa)	C_{55} (GPa)	C_{66} (GPa)
4	200	68.5	58.1	48.6	38.8	27.2	31.6	10.2	14.3	11.2
	300	67.4	56.1	48.6	35.8	26.9	31.2	10.1	13.9	11.6
	400	64.4	55.2	45.9	33.4	26.3	29.1	9.6	13.2	11.7
	450	65.3	55.4	46.4	33.8	27.3	30.6	9.6	13.5	12.1
5	200	79.4	67.3	57.0	45.2	34.3	37.8	11.9	16.5	12.6
	300	77.5	65.8	55.3	44.6	32.8	37.0	11.4	15.6	12.8
	400	74.5	64.0	54.8	40.3	32.9	35.6	11.3	15.2	13.0
	450	74.6	63.9	54.7	40.7	33.2	35.1	11.3	14.9	13.2
	500	72.6	62.0	54.0	39.2	31.9	33.6	10.7	14.7	13.3
6	200	88.1	74.4	64.4	52.2	39.1	42.7	13.6	18.2	13.6
	300	85.8	73.0	63.4	49.4	38.8	41.3	13.1	17.4	14.0
	400	83.4	71.9	63.8	46.3	38.8	40.1	12.6	16.9	14.3
	450	83.8	72.2	62.0	46.8	38.8	40.9	12.6	16.8	14.4
	500	81.0	70.5	60.2	46.7	37.6	39.4	12.1	16.1	14.2
7	200	96.4	81.5	71.2	58.1	44.2	48.2	15.3	19.8	14.7
	300	93.5	79.9	69.6	54.9	43.2	46.4	14.5	19.0	15.1
	400	91.0	79.4	69.7	53.5	42.5	45.0	13.7	18.4	15.2
	450	91.0	78.1	67.4	53.1	42.7	45.2	13.6	18.2	15.3
	500	89.6	77.6	68.2	51.6	43.0	44.8	13.5	17.9	15.5
8	200	102.7	88.5	77.6	62.0	48.7	51.9	16.2	21.3	16.0
	300	101.6	88.5	77.8	61.4	48.5	51.6	15.6	20.7	16.3
	400	99.1	86.2	77.0	57.6	48.5	50.6	15.0	19.7	16.3
	450	99.9	85.5	76.0	57.7	48.5	51.1	15.0	19.8	16.5
	500	97.9	85.0	75.1	57.5	47.0	49.9	14.8	19.3	16.5
	550	97.1	83.7	73.0	56.2	47.1	49.0	14.2	18.8	16.4
9	200	112.0	96.0	87.0	68.1	54.7	58.4	17.5	23.1	17.5
	300	109.4	94.0	84.9	65.5	53.5	57.1	17.0	22.2	17.3
	400	107.5	93.7	83.4	63.9	53.2	55.7	16.0	21.5	17.6
	450	106.4	92.4	82.9	63.2	53.0	55.5	15.8	20.9	17.4
	500	106.4	92.1	82.7	63.4	52.9	55.7	15.8	20.7	17.4
	550	105.3	91.7	81.5	62.8	53.3	55.3	15.3	20.1	17.5
10	200	118.6	100.7	91.6	73.0	58.6	62.9	18.8	23.9	18.0
	300	117.4	102.2	93.7	72.3	58.8	62.1	17.6	23.6	18.5
	400	116.2	101.0	90.4	71.0	58.5	61.7	17.2	22.8	18.5
	450	113.9	98.5	88.8	68.5	57.5	60.2	16.9	22.4	18.5
	500	112.3	97.8	87.9	68.4	57.2	59.6	16.5	21.7	18.3
	550	112.5	98.2	87.7	68.7	56.5	59.5	16.4	21.8	18.6
11	200	126.6	108.4	100.4	80.0	63.8	69.3	20.0	25.6	18.8
	300	125.6	108.2	99.0	77.8	64.3	67.8	18.7	24.7	19.3
	400	120.9	106.9	97.2	76.1	61.7	65.6	18.1	23.8	19.3
	450	120.6	105.1	93.5	74.5	61.6	65.0	17.5	23.3	19.1
	500	120.6	104.6	94.1	74.5	61.8	64.7	17.8	22.9	18.8
	550	119.8	104.4	92.5	74.1	61.2	65.0	17.2	22.8	19.3

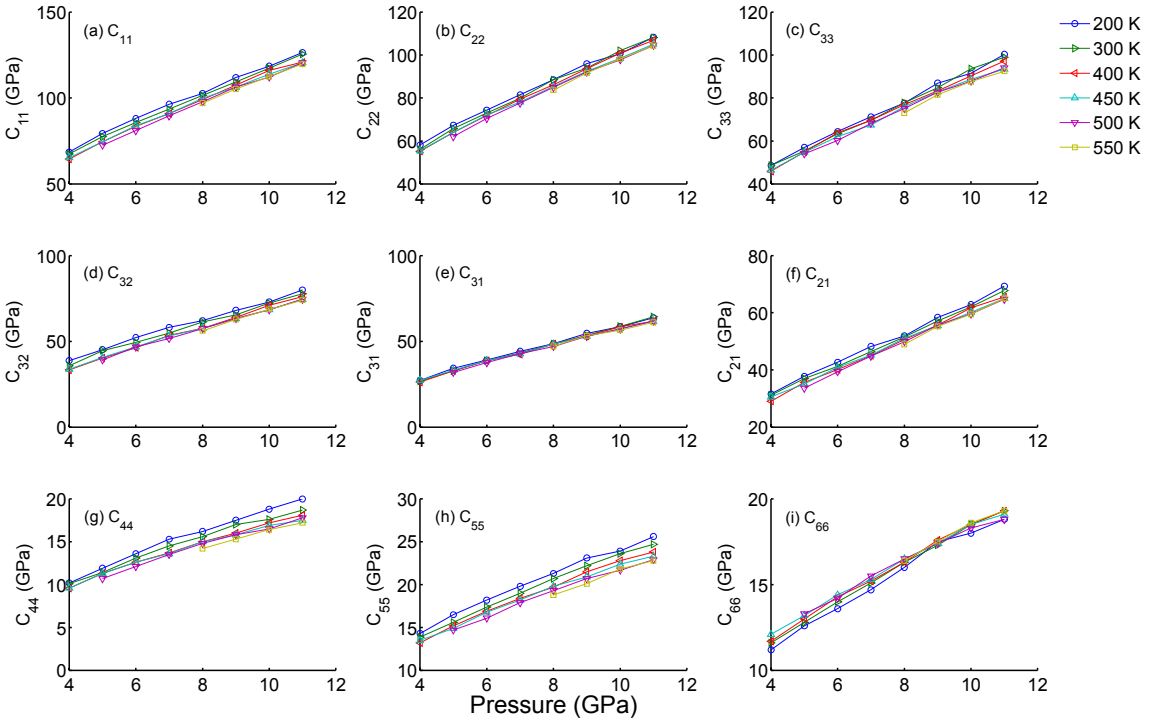

Fig.1 Variation of the components of the elasticity tensor with pressure for various temperatures

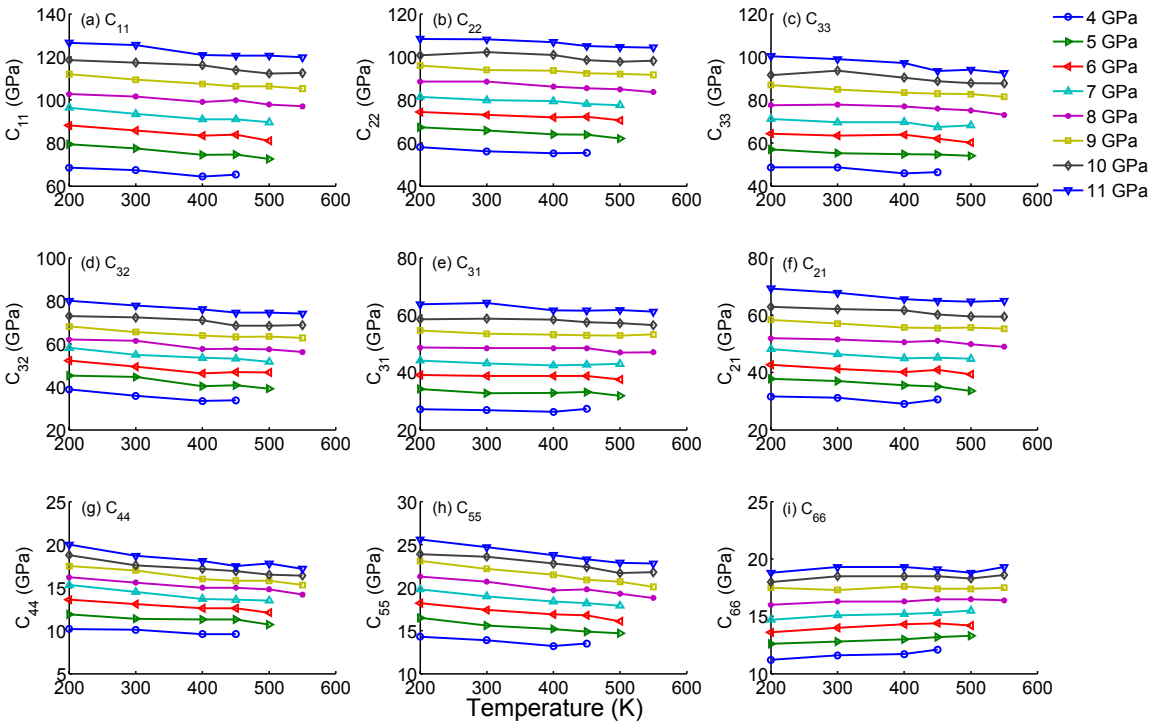

Fig.2 Variation of the components of the elasticity tensor with temperature for various pressures

From Figs. 1 and 2, it is evident that the anisotropic nature of RDX is preserved in the γ-polymorph across the simulated range of pressures and temperatures. Further, it also behaves as an orthotropic material with negligible dependence of any normal stress/strain on any shear stress/strain and that of a shear stress/strain along one direction on the shear stress/strain in the other directions. A direct comparison of the variation of the elastic moduli with pressure and temperature indicates the strong sensitivity of all elastic moduli with pressure. The variation with temperature is small in the simulated range. γ-RDX exhibits monotonic increase in stiffness with pressure, and slight softening with temperature. The elastic moduli are fitted to a linear function in pressure and temperature given by,

$$C_{ij} = c_0 + c_1 p + c_2 T, \quad (6)$$

where i and j are the indices in Voigt notation. The constants, c_0, c_1, and c_2 for the nine components of elastic modulus tensor are given in Table 4.

Table 4 Constants in the linear fit for elastic moduli

	c_0 (GPa)	c_1	c_2 (GPa/K)
C_{11}	42.44	8.05	-0.019
C_{22}	33.32	7.16	-0.012
C_{33}	24.97	7.06	-0.014
C_{32}	19.20	5.84	-0.018
C_{31}	9.56	5.04	-0.005
C_{21}	13.69	5.16	-0.010
C_{44}	7.36	1.22	-0.006
C_{55}	10.48	1.50	-0.007
C_{66}	7.15	1.06	0.002

A comparison with α-RDX shows that the hardening of γ-RDX with pressure correlates with a similar hardening of α-RDX[9] reported in literature. Also, the hardening rate of RDX increases with pressure, for both the α-[9] and γ-polymorphs. Finally, the softening of γ-RDX with temperature follows a similar trend observed in α-RDX.[9]

3.2 pVT equation of state and derived parameters

In the present analysis, the variation of lattice constants and volume of the system with pressure and temperature are studied for γ-RDX. We first validate the calculated lattice constants and volume of the unit cell of γ-RDX at 5.2 GPa and 300 K with experimental observations[29] and verify with the simulation[24] results as shown in Table 5.

Table 5 Lattice constants for γ-RDX at 5.2 GPa and 300 K

	Davidson et al.[a]	Munday et al.[b]	Calculated
a (Å)	12.565	12.69	12.71
b (Å)	10.930	11.06	11.05
c (Å)	9.477	9.64	9.64
Volume (Å^3)	1301.5	1353.3	1354.9

[a] Reference 29; [b] Reference 24

In Fig. 3, we compare the lattice constants of γ-RDX at 300 K with the experimental[29] and previous simulation data[24] as a function of pressure. The present simulation results compare well with those presented in Munday et al.[24]

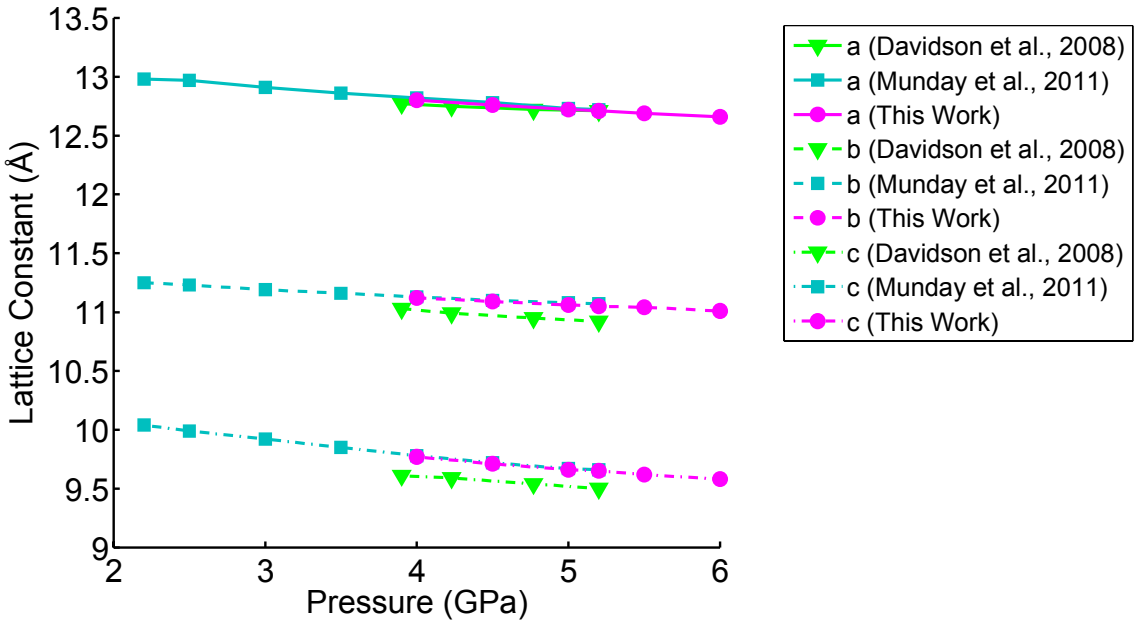

Fig. 3 Variation of lattice constants with pressure at 300 K for γ-RDX

The variation of the lattice constants and volume of the system for γ-RDX is tabulated in Table 6 for the pressure ranging from 4 GPa to 11 GPa and temperature range of 200K to 550 K. Figs. 4 and 5 depict the variation of the lattice constants and volume with pressure and temperature, respectively.

We observe that the b-lattice direction is rather insensitive to temperature changes and is almost unchanged at higher pressures. This can be due to the reduction in volume and hence high density at high pressures. The variation of lattice constants and volume of γ-RDX with pressure and temperature follow a trend qualitatively similar to that of α-RDX.[9]

Table 6 Variation of lattice constants and volume of system with pressure and temperature for γ-RDX

P (GPa)	T (K)	a (Å)	b (Å)	c (Å)	Volume (Å^3)
4	200	12.78	11.10	9.74	1382.7
	250	12.79	11.11	9.75	1386.6
	300	12.80	11.12	9.77	1390.5
	350	12.81	11.13	9.78	1394.5
	400	12.83	11.13	9.80	1398.8
	450	12.84	11.14	9.81	1402.8
5	200	12.70	11.05	9.64	1353.4
	250	12.71	11.06	9.65	1357.0
	300	12.72	11.06	9.66	1360.5
	350	12.73	11.07	9.68	1364.2
	400	12.74	11.07	9.69	1367.6
	450	12.75	11.08	9.70	1371.0
	500	12.76	11.09	9.72	1374.9
6	200	12.64	11.01	9.55	1328.6
	250	12.65	11.01	9.56	1331.8
	300	12.66	11.01	9.58	1334.9
	350	12.67	11.02	9.59	1337.9
	400	12.67	11.02	9.60	1341.3
	450	12.68	11.02	9.61	1344.4
	500	12.69	11.03	9.63	1348.0
7	200	12.58	10.97	9.48	1306.9
	250	12.59	10.97	9.49	1309.8
	300	12.60	10.97	9.50	1312.7
	350	12.60	10.97	9.51	1315.5
	400	12.61	10.97	9.53	1318.4
	450	12.62	10.97	9.54	1321.4
	500	12.63	10.97	9.55	1324.3
8	200	12.52	10.92	9.41	1287.6
	250	12.53	10.92	9.43	1290.3
	300	12.54	10.92	9.44	1292.8
	350	12.55	10.93	9.45	1295.4
	400	12.56	10.93	9.46	1298.3
	450	12.57	10.93	9.47	1300.8
	500	12.57	10.93	9.48	1303.5
	550	12.58	10.93	9.50	1306.2
9	200	12.47	10.88	9.36	1270.4
	250	12.48	10.88	9.37	1272.7
	300	12.49	10.88	9.38	1275.2
	350	12.50	10.88	9.39	1277.4
	400	12.51	10.89	9.40	1279.9
	450	12.52	10.89	9.41	1282.4
	500	12.52	10.89	9.42	1284.9
	550	12.53	10.89	9.43	1287.4
10	200	12.43	10.85	9.31	1254.5
	250	12.43	10.85	9.32	1256.7
	300	12.44	10.85	9.33	1258.8
	350	12.45	10.85	9.34	1261.1
	400	12.46	10.85	9.35	1263.3
	450	12.47	10.85	9.36	1265.7
	500	12.48	10.85	9.37	1267.9
	550	12.48	10.85	9.38	1270.2
11	200	12.38	10.81	9.26	1239.8
	250	12.39	10.81	9.27	1241.9
	300	12.40	10.81	9.28	1244.0
	350	12.41	10.81	9.29	1246.1
	400	12.42	10.81	9.30	1248.3
	450	12.42	10.81	9.31	1250.4
	500	12.43	10.81	9.32	1252.5
	550	12.44	10.81	9.33	1254.5

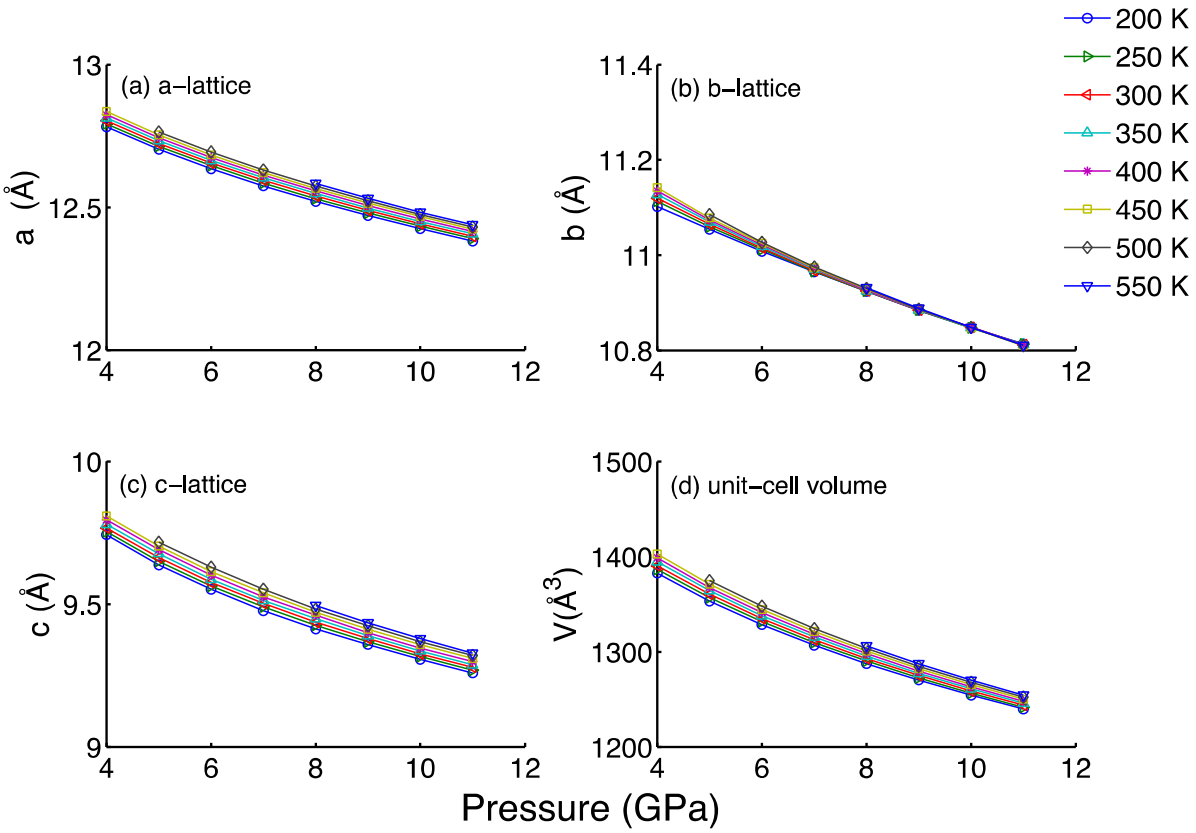

Fig. 4 Variation of lattice constants and volume with pressure for various temperatures

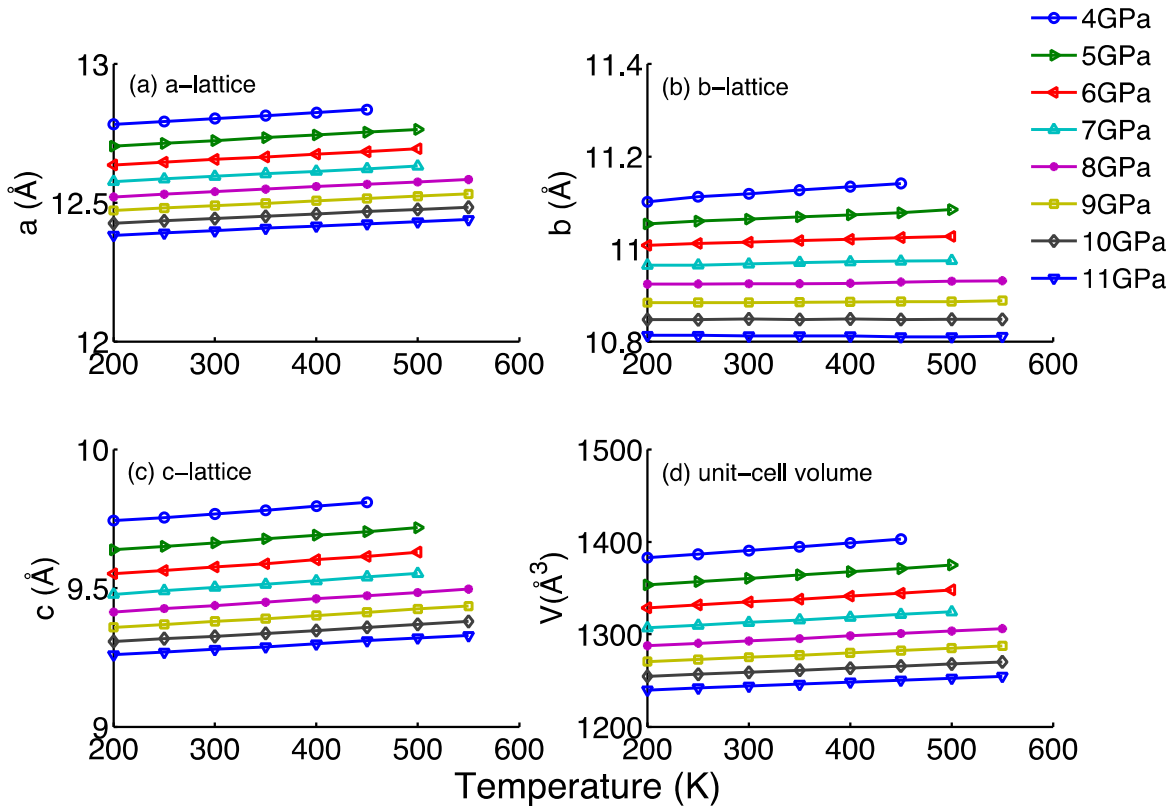

Fig. 5 Variation of lattice constants and volume with temperature for various pressures

A third order Birch-Murnaghan equation of state[34] is obtained using least squares method for γ-RDX at various temperatures. The general form of the equation at a given temperature is,

$$p(V)=\frac{3B_0}{2}\left[\left(\frac{V_0}{V}\right)^{\frac{7}{3}}-\left(\frac{V_0}{V}\right)^{\frac{5}{3}}\right]\left\{1+\frac{3}{4}(B_0'-4)\left[\left(\frac{V_0}{V}\right)^{\frac{2}{3}}-1\right]\right\}, \quad (7)$$

where B_0 is the bulk modulus of the material at 0 Pa, B_0' is the derivative of bulk modulus with respect to pressure at 0 Pa, and V_0 is the volume of the system at 0 Pa. These constants are given in Table 7 for the entire temperature range of the simulations.

Table 7 Constants in the Birch Murnaghan equation of state

Temperature (K)	B_0 (GPa)	B_0'	V_0 (Å^3)
200	6.4	18.2	1658.4
250	6.3	18.0	1668.0
300	5.7	18.9	1682.5
350	2.4	36.8	1739.5
400	1.4	56.9	1769.1
450	1.0	73.3	1787.2
500	1.4	52.7	1790.9
550	10.2	11.1	1668.8

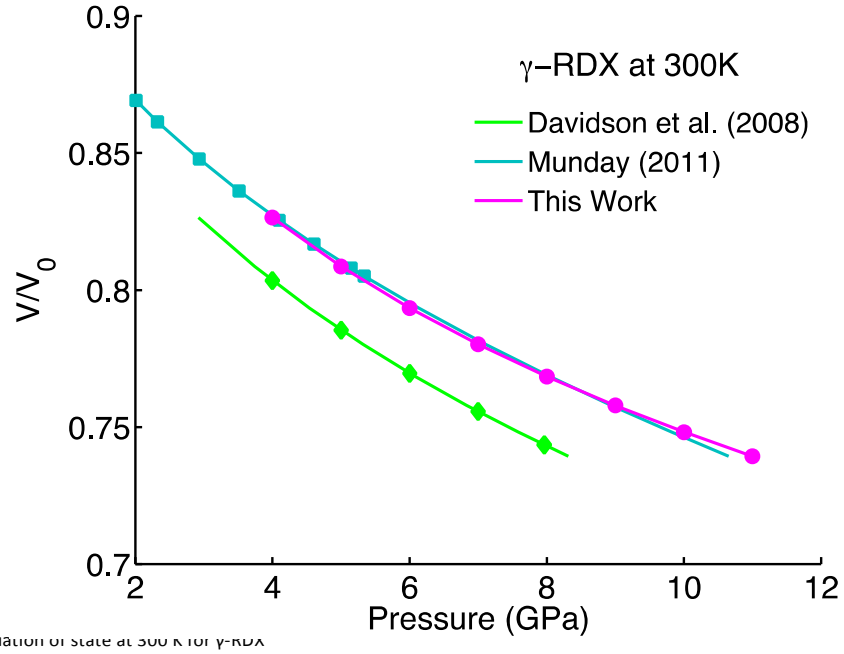

Fig. 6 Birch Murnaghan equation of state at 300 K for γ-RDX

The constants at 500 K and 550 K are obtained using lesser data points since γ-RDX is stable for a short range of pressure for these temperatures. Hence, they show deviation from the general trend of the constants with temperature.

In Fig. 6, we compare the Birch-Murnaghan equation of state (Eq. (7)) for our data along with the experimental results,[29] and previous simulation results.[32] From the plots for the equation of state for Munday's simulation[32] and the present simulation, we can conclude that they represent approximately the same relation between pressure and volume for γ-RDX. The present simulation over-predicts the volume of the system when compared with experimental results.[29] This is also evident from the volume of the system calculated at 5.2 GPa and 300 K.

The coefficients of thermal expansion along all three lattice directions and the volumetric coefficient of expansion are calculated using the reference temperature as 300 K. On observation of the variation of the lattice constants and volume with temperature, a linear fit is deemed to be sufficient to calculate the coefficients of thermal expansion. The coefficients of thermal expansion and their variation with pressure are presented in Table 8 and Fig. 7.

Table 8 Variation of coefficients of thermal expansion with pressure

P (GPa)	α_x ($\times10^{-5}$) (K^{-1})	α_y ($\times10^{-5}$) (K^{-1})	α_z ($\times10^{-5}$) (K^{-1})	γ ($\times10^{-5}$) (K^{-1})
4	1.67	1.40	2.73	5.80
5	1.59	0.90	2.75	5.23
6	1.53	0.58	2.69	4.81
7	1.47	0.33	2.61	4.41
8	1.42	0.20	2.48	4.11
9	1.36	0.11	2.33	3.81
10	1.33	0.02	2.22	3.57
11	1.31	--	2.16	3.39

The pVT data and the Birch Murnaghan equation of state are useful as they allow incorporating the response of γ-RDX in

mesoscale and continuum modeling. The coefficients of thermal expansion of γ-RDX remain orthotropic with variation in pressure and temperature. In comparison to α-RDX,[9] they exhibit negligible variation with pressure. The coefficients of thermal expansion of α-RDX[9] are smaller than those of γ-RDX around the α-γ phase transition pressure at 4 GPa. Furthermore, the reduction in volume during phase change and the high pressures lead to high density, which shows significant effect on thermal expansion.

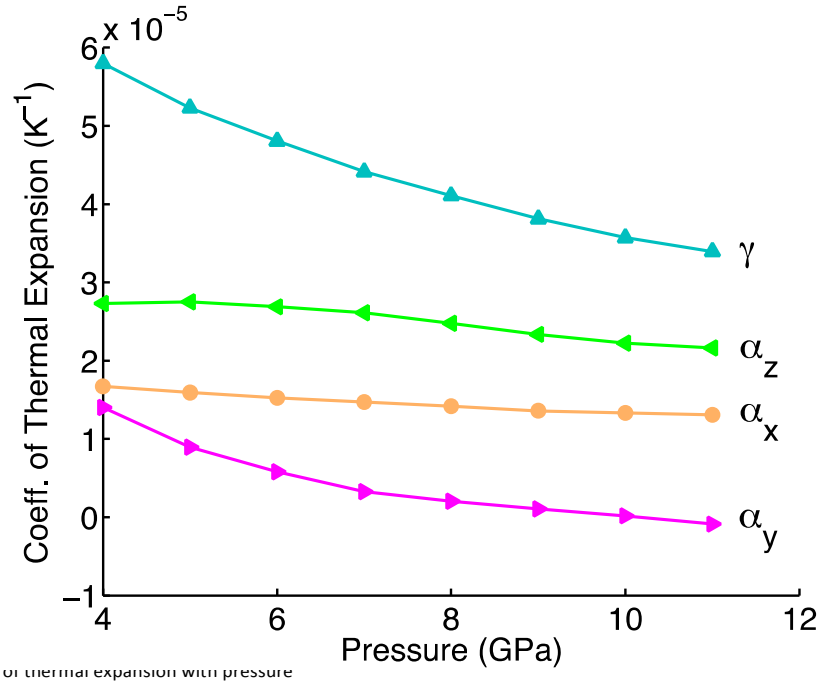

Fig. 7 Variation of coefficients of thermal expansion with pressure

3.3 Discussion

A common factor underpinning the observed trends in the elastic modulus tensor and coefficient of thermal expansion for γ-RDX is the increasing resistance of the material to thermomechanical stimuli with pressure. At high pressures, we observe that γ-RDX becomes more difficult to deform through stress or temperature as indicated by the hardening of the material and decrease in the coefficients of thermal expansion with pressure. The elastic modulus tensor indicates the change in the intermolecular forces with changing intermolecular spacing. The hardening of γ-RDX indicates that the intermolecular forces increase rapidly with increasing pressure, suggesting stronger intermolecular interactions at higher pressures. The coefficient of thermal expansion indicates the change in the mean intermolecular spacing with temperature. The decrease in coefficient of thermal expansion with pressure indicates a much steeper intermolecular potential at higher pressures. A steeper potential results in stronger intermolecular forces and would have significant influence on the detonation sensitivity of the material at high pressures. It should be noted that these observations are only indicative of the behavior of γ-RDX to thermomechanical stimuli. Nevertheless, the present study is an important preliminary step in simulating more complex molecular and continuum scale simulations on the thermomechanical response of γ-RDX.

4. Concluding Remarks

A detailed study of the thermomechanical properties of γ-RDX has been undertaken using molecular dynamics simulations with the non-reactive fully flexible Smith and Bharadwaj (SB) molecular potential. The potential has been shown to yield consistent results across a range of pressures and temperatures. The anisotropic elastic modulus tensor has been derived as a function of temperature and pressure for a wide range of conditions in which γ-RDX is known to be stable. An additional outcome of the calculation is the pVT data from which the equation of state and coefficients of thermal expansion have been obtained.

The calculated elastic moduli and lattice constants of γ-RDX at 5.2 GPa pressure and 300 K temperature are in good agreement with existing simulation and experimental results, with an error of 3% and 2% or less, respectively. The elastic moduli exhibit strong sensitivity to variations in pressure and negligible variation with respect to temperature within the simulated range of thermodynamic states, resulting in monotonically increase in stiffness with pressure and slight softening with temperature. The lattice constants show linear variation with temperature. We observe that among the lattice directions, the b-lattice direction is insensitive to temperature changes particularly at higher pressures. The variation of elastic moduli and lattice constants of γ-RDX with pressure and temperature follow a similar trend as that of α-polymorph. The

variation of lattice constants and volume with temperature is very similar at any pressure. This is clearly indicated in the negligible change of the three linear and the volumetric coefficients of thermal expansion with pressure. The coefficients of thermal expansion of γ-RDX are found to be greater than those of α-RDX around the α-γ phase transition pressure. The reduction in volume during phase change shows great effect on thermal expansion.

In the absence of experimental data, the present study provides a foundation to analyze macroscopic response of γ-RDX at the continuum level. The accurate prediction of the elastic moduli along with their trends with pressure and temperature, the equation of state, and other properties like coefficient of thermal expansion, are crucial for the development of physically based constitutive models for RDX. These models are an important component in the accurate prediction of the thermomechanical response of γ-RDX. The material and crystallographic parameters along with the equation of state of γ-RDX will also be instrumental in understanding and predicting the effects of anisotropic deformation and phase transformation on the initiation and the critical parameters for transition to detonation in RDX under intended or unintended thermomechanical stimuli.

The SB potential has resulted in a stable simulation system and consistent output in the diverse range of conditions that is applied in the present study. Therefore, this study demonstrates the stability of the SB potential for quasi-static thermomechanical loading of γ-RDX. A natural next step would be to examine the response due to shock loading on γ-RDX using this potential. Other material and crystallographic information such as slip systems, response to shock and indentation loads for γ-RDX, and α-γ phase interfacial properties need further investigation.

Acknowledgement

This work has been supported in part by the Office of Naval Research (ONR) grants N000140810462 and N000141210527 with Dr. Cliff Bedford as the cognizant program manager.

References

1 S. De, A. R. Zamiri, and Rahul, *J. Mech. Phys. Solids*, 2013, **64**, 287-301.
2 J. D. Clayton, and R. Becker, *J. Appl. Phys. (Melville, NY, U. S.)*, 2012, **111**, 063512.
3 R. J. Clifton, in *Shock Waves and the Mechanical Properties of Solids*, ed. J. J. Burke and V. Weiss, Syracuse University Press, Syracuse, N.Y., 1971, pp. 73-116.
4 J. M. Winey, and Y. M. Gupta, *J. Appl. Phys. (Melville, NY, U. S.)*, 2004, **96**, 1993-1999.
5 J. M. Winey, and Y. M. Gupta, *J. Appl. Phys. (Melville, NY, U. S.)*, 2006, **99**, 023510.
6 R. B. Schwarz, D. E. Hooks, J. J. Dick, J. I. Archuleta, and A. R. Martinez, *J. Appl. Phys. (Melville, NY, U. S.)*, 2005, **98**, 056106.
7 J. J. Haycraft, L. L. Stevens, and C. J. Eckhardt, *J. Chem. Phys.*, 2006, **124**, 024712.
8 B. Sun, J. M. Winey, N. Hemmi, Z. A. Dreger, K. A. Zimmerman, Y. M. Gupta, D. H. Torchinsky, and K. A. Nelson, *J. Appl. Phys. (Melville, NY, U. S.)*, 2008, **104**, 073517.
9 T. D. Sewell, and C. M. Bennett, *J. Appl. Phys. (Melville, NY, U. S.)*, 2000, **88**, 88-95.
10 J. J. Haycraft, L. L. Stevens, and C. J. Eckhardt, *J. Appl. Phys. (Melville, NY, U. S.)*, 2006, **100**, 053508.
11 S. Haussühl, *Z. Kristallogr.*, 2001, **216**, 339-353.
12 J. E. Patterson, Z. A. Dreger, and Y. M. Gupta, *J. Phys. Chem. B*, 2007, **111**, 10897-10904.
13 N. C. Dang, Z. A. Dreger, Y. M. Gupta, and D. E. Hooks, *J. Phys. Chem. A*, 2010, **114**, 11560-11566.
14 Z. A. Dreger, and Y. M. Gupta, *J. Phys. Chem. A*, 2012, **116**, 8713-8717.
15 P. Politzer, J. S. Murray, in *Advances in Quantum Chemistry*, ed. J. R. Sabin, Academic Press, 2014, vol. 69, ch. 1, pp. 1-30.
16 P. Politzer, and J. S. Murray, *Cent. Eur. J. Energ. Mater.*, 2011, **8**, 209-220.
17 S. Boyd, J. S. Murray, and P. Politzer, *J. Chem. Phys.*, 2009, **131**, 204903.
18 R. W. Armstrong, C. S. Coffey, V.F. DeVost, and W. L. Elban, *J. Appl. Phys. (Melville, NY, U. S.)*, 1990, **68**, 979-984.
19 C. S. Choi, and E. Prince, *Acta Crystallogr., Sect. B: Struct. Crystallogr. Cryst. Chem.*, 1972, **28**, 2857-2862.
20 H. H. Cady, *J. Chem. Eng. Data*, 1972, **17**, 369-371.
21 M. J. Cawkwell, K. J. Ramos, D. E. Hooks, and T. D. Sewell, *J. Appl. Phys. (Melville, NY, U. S.)*, 2010, **107**, 063512.
22 K. J. Ramos, D. E. Hooks, T. D. Sewell, and M. J. Cawkwell, *J. Appl. Phys. (Melville, NY, U. S.)*, 2010, **108**, 066105.
23 G. D. Smith, and R. K. Bharadwaj, *J. Phys. Chem. B*, 1999, **103**, 3570-3575.
24 L. B. Munday, P. W. Chung, B. M. Rice, and S. D. Solares, *J. Phys. Chem. B*, 2011, **115**, 4378-4386.
25 D. Bedrov, J. B. Hooper, G. D. Smith, and T. D. Sewell, *J. Chem. Phys.*, 2009, **131**, 034712.
26 D. C. Sorescu, B. M. Rice, and D. L. Thompson, *J. Phys. Chem. B*, 1997, **101**, 798-808.
27 Z. A. Dreger, and Y. M. Gupta, *J. Phys. Chem. A*, 2010, **114**, 8099-8105.
28 B. J. Baer, J. Oxley, and M. Nicol, *High Pressure Res.*, 1990, **2**, 99-108.
29 A. J. Davidson, I. D. Oswald, D. J. Francis, A. R. Lennie, W. G. Marshall, D. I. Millar, C. R. Pulham, J. E. Warrenc, and A. S. Cumming, *CrystEngComm*, 2008, **10**, 162-165.
30 M. J. Cawkwell, T. D. Sewell, L. Zheng, and D. L. Thompson, *Phys. Rev. B: Condens. Matter Mater. Phys.*, 2008, **78**, 014107.
31 D. Bedrov, C. Ayyagari, G. D. Smith, T. D. Sewell, R. Menikoff, and J. M. Zaug, *J. Comput.-Aided Mater. Des.*, 2001, **8**, 77-85.
32 L. B. Munday, Ph. D. Thesis, University of Maryland, 2011. http://hdl.handle.net/1903/12254
33 S. Plimpton, *J. Comput. Phys.*, 1995, **117**, 1-19. http://lammps.sandia.gov
34 F. Birch, *Phys. Rev.*, 1947, **71**, 809-824.